JACS
JOURNAL OF THE AMERICAN CHEMICAL SOCIETY
Article
Cite This: J. Am. Chem. Soc. 2019, 141, 13212−13221
pubs.acs.org/JACS

Mechanistic Study of Oxygen Reduction at Liquid/Liquid Interfaces by Hybrid Ultramicroelectrodes and Mass Spectrometry

Chaoyue Gu,[†] Xin Nie,[†] Jiezhang Jiang,[†] Zifei Chen,[†] Yifan Dong,[†] Xin Zhang,[†] Junjie Liu,[†] Zhengyou Yu,[†] Zhiwei Zhu,[†] Jian Liu,[†] Xiaoyun Liu,[‡] and Yuanhua Shao*[,†]

[†]Beijing National Laboratory for Molecular Sciences, College of Chemistry and Molecular Engineering, Peking University, Beijing 100871, China

[‡]Department of Microbiology, School of Basic Medical Sciences, Peking University Health Science Center, Beijing 100191, China

Supporting Information

ABSTRACT: Proton-coupled electron transfer (PCET) reactions at various interfaces (liquid/membrane, solid/electrolyte, liquid/liquid) lie at the heart of many processes in biology and chemistry. Mechanistic study can provide profound understanding of PCET and rational design of new systems. However, most mechanisms of PCET reactions at a liquid/liquid interface have been proposed based on electrochemical and spectroscopic data, which lack direct evidence for possible intermediates. Moreover, a liquid/liquid interface as one type of soft interface is dynamic, making the investigation of interfacial reactions very challenging. Herein a novel electrochemistry method coupled to mass spectrometry (EC-MS) was introduced for in situ study of the oxygen reduction reaction (ORR) by ferrocene (Fc) under catalysis from cobalt tetraphenylporphine (CoTPP) at liquid/liquid interfaces. The key units are two types of gel hybrid ultramicroelectrodes (agar-gel/organic hybrid ultramicroelectrodes and water/PVC-gel hybrid ultramicroelectrodes), which were made based on dual micro- or nanopipettes. A solidified liquid/liquid interface can be formed at the tip of these pipettes, and it serves as both an electrochemical cell and a nanospray emitter for mass spectrometry. We demonstrated that the solidified L/L interfaces were very similar to typical L/L interfaces. Key CoTPP intermediates of the ORR at the liquid/liquid interfaces were identified for the first time, and the four-electron oxygen reduction pathway predominated, which provides valuable insights into the mechanism of the ORR. Theoretical simulation has further supported the possibility of formation of intermediates. This type of platform is promising for in situ tracking and identifying intermediates to study complicated reactions at liquid/liquid interfaces or other soft interfaces.

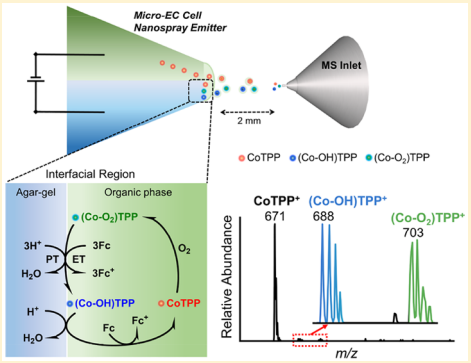

INTRODUCTION

Proton-coupled electron transfer (PCET) reactions are one of the most fundamental processes in biology and chemistry.[1−3] The reactions are closely related to many important processes, such as photosynthesis,[4,5] respiration,[6,7] energy conversion, and storage.[8−16] Several of these processes are major challenges in sustainable chemistry, for example splitting water with high efficiency. A liquid/liquid (L/L) interface, where charge (electron and ion) transfer reactions can occur,[17] has drawn considerable attention in the past few decades.[18−20] This is because of its biomimetic features to function as a simple model of biological membranes,[21−23] and various applications in chemistry, including chemical sensors,[24] phase-transfer catalysis,[25] ion extraction,[26] and drug release.[27,28] In addition, the L/L interfaces are rather suitable to study PCET reactions with a proton source in the aqueous phase and lipophilic electron donors in the organic phase. Therefore, an in-depth understanding of the PCET reactions at L/L interfaces is urgently needed. Plenty of electrochemical techniques, such as cyclic voltammetry,[29,30] rotating disk electrodes,[31] and impedance,[32] have been employed to decipher the performance of the PCET reactions at an L/L interface. Additionally, spectroscopic techniques have also been used to deal with spectral changes during PCET reactions.[33] Despite the existence of these tools, a direct method for identification of the intermediates in the PCET reactions is still lacking, which is essential to explain the mechanism of a PCET reaction. Compared with these aforementioned approaches, mass spectrometry possesses high sensitivity and chemical specificity toward electrochemical intermediates or products. Electrochemistry coupling to MS (EC-MS) has attracted increasing attention in recent years, because it can provide the molecular weight and structural discrimination about products and intermediates in the EC reactions and systems.[34] Thus, the combination of them could produce a powerful technique for the study of complicated EC or interfacial reactions.

The combination of EC with mass spectrometry (MS) was first introduced by Bruckenstein et al. in 1971.[35] So far, it has been rapidly developed in intermediates detection and mechanism study toward EC reactions. Chen and Zare et al.

Received: June 13, 2019
Published: July 28, 2019

DOI: 10.1021/jacs.9b06299
J. Am. Chem. Soc. 2019, 141, 13212−13221

have recently developed a wheel electrode, coupling to DESI-MS to identity diimines and *N*,*N*-dimethylaniline radical intermediates of EC reactions.[36,37] Luo and Shao et al. have employed a carbon hybrid ultramicroelectrode as the micro-electrochemical cell and an MS emitter to capture the intermediates for further illuminating the mechanisms of the electrochemiluminescent processes and other EC reactions.[38] MS is not only a powerful tool for studying reactions at a solid/electrolyte interface but also useful for systems at an L/L interface. Using biphasic electrospray ionization mass spectrometry, metal ion complexes at the L/L interfaces were detected by Girault et al.[39] and Stockmann et al.[40] Besides, ex situ EC-MS was implemented to characterize the tertiary structure of electroadsorbed lysozyme at soft interfaces.[41] Liu et al. utilized microchips as electrochemical cells to study L/L interfaces by MS, but they could only monitor the mixtures of both phases.[42] Up to now, however, it is still very challenging for in situ study of interfacial reactions at L/L interfaces by EC-MS. First, for the relatively long distance between the existing electrochemical cells and mass spectrometer inlet, the products or intermediates generated at the L/L interfaces could not be delivered to the mass spectrometer immediately, making the detection of short-lived analytes difficult. Second, owing to the dynamic nature of the L/L interfaces, monitoring only the EC reactions at L/L interfaces becomes very difficult, e.g., the two phases would emit into the mass spectrometer together and detection in the mass spectrometer is the mixture of both phases. Thus, it is very difficult to identify the intermediates produced only in the interfacial reactions using the existing setups.

In this work, we developed an EC-MS technique based on dual micropipettes, which could be used to investigate the interfacial reactions at an L/L interface (Scheme 1). In this setup, one channel was solidified as an agar-gel or a PVC-gel microelectrode, and the other could be filled with organic or aqueous phases. Thus, agar-gel/organic (O) interfaces and water (W)/PVC-gel interfaces were formed at the tip of the dual microelectrodes, which were analogous to micro/nano-W/O interfaces. The Ag/AgCl electrode and Ag/AgTPBF$_5$ electrode were inserted into the aqueous or agar-gel barrel and organic or PVC-gel barrel, respectively. With a suitable potential applied, the gel hybrid ultramicroelectrode served as an electrochemical cell where the electrochemical reaction could take place. By triggering the piezoelectric pistol, which could apply a pulsed voltage at the back of the microcell, primary ion flow was generated to induce the solution of products and intermediates at the interfacial layer spraying into the mass spectrometer to be analyzed.[43] This piezoelectric pistol has negligible influence on the EC system because they do not touch each other (see Scheme 1). During the whole process, the agar-gel/O or W/PVC-gel interfaces were stable enough because of the gel property of agar for the aqueous phase or the PVC for the organic phase, making one phase fairly fixed, and only the substances (reactants, intermediates, or products) at the interfacial layer could enter the mass spectrometer. The distance between the electrode surface and the mass spectrometer inlet was quite short (ca. 2 mm), which reduced the delay time between electrochemical reaction and detection, making the determination of highly reactive intermediates possible.

Using this novel EC-MS technique, the mechanism of molecular electrocatalysis for the oxygen reduction reaction (ORR) proceeding via PCET processes at the agar-gel/O or

Scheme 1. (a) Experimental Setup.[a] (b) Proposed Mechanism of ORR Consisting of H^+ in Agar-Gel and Fc in Organic Phase Catalyzed by CoTPP, in Which the Proton Transfer (PT) and Electron Transfer (ET) Are Coupled at the L/L Interface

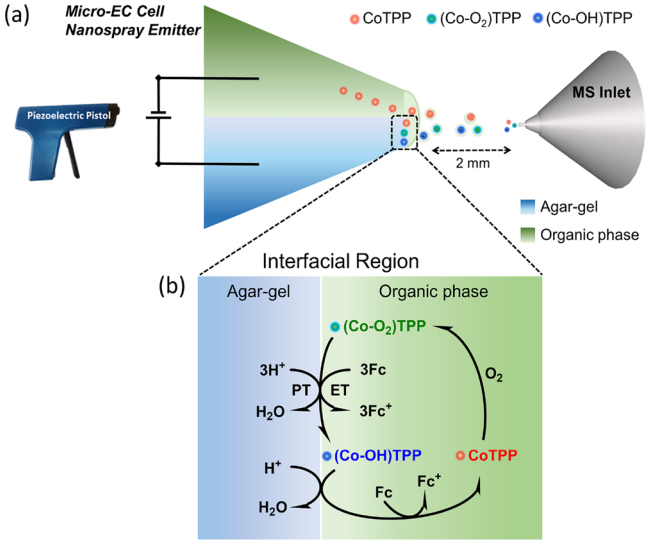

[a]The gel hybrid ultramicroelectrode functioned as the micro-EC cell/nanospray emitter (only the agar-gel/O hybrid ultramicroelectrode is shown). A piezoelectric pistol was applied to induce spray from the micropipettes with ∼1.5 μm diameter tip, making the solution at the L/L interface spray into the mass spectrometer.

PVC-gel/W interfaces was studied to confirm the proposed mechanism as shown in Scheme 1 (only the four-electron pathway is shown).[44] This oxygen reduction involved protons in the aqueous phase or pseudoaqueous phase and electron donor ferrocene (Fc) in the organic phase in the presence of cobalt tetraphenylporphine (CoTPP) as the ORR molecular catalyst. Here the transfer of protons, electron, and Fc^+ during the ORR occurring at the L/L interfaces were recorded by cyclic voltammetry, and the results elucidated that the solidified L/L interfaces were very similar to the conventional L/L interfaces. Using the EC-MS technique, the key intermediates (Co−O_2)TPP and (Co−OH)TPP produced at the L/L interface were in situ studied for the first time, in contrast to the detection of two-phase mixtures. Theoretical simulation was performed to further confirm the possibility of formation of the (Co−O_2)TPP and (Co−OH)TPP intermediates. Combining the macro-biphasic reactions with spectroscopy, during which the interfacial polarization was controlled by the partition of the common ion without external voltage, the main four-electron oxygen reduction pathway was proposed.

EXPERIMENTAL SECTION

Chemicals. Ferrocene (Fc, 98%), lithium chloride (LiCl, >97%), potassium chloride (KCl, >99.5%), sulfuric acid (H_2SO_4, 98%), and 1,2-dichloroethane (DCE, ≥99%) were purchased from Beijing Chemical Company. 5,10,15,20-*meso*-Tetraphenylporphyrin cobalt (CoTPP, 98%) was supplied by Tokyo Chemical Industry. Agar (ash <1.5%), polyvinyl chloride (PVC, K-value 72−71), sodium iodide (NaI, >99.5%), and trifluoroacetic acid (TFA, 99.9%) were supplied by Macklin. Tetramethylammonium chloride (TMACl, ≥99.0%), lithium tetra(pentafluorophenyl)borate (LiTPBF$_5$), and potassium tetrakis(4-chlorophenyl)borate (KTPBCl, ≥98%) were purchased from Fluka. Dibenzo-18-crown-6 (DB18C6, >98%) was

DOI: 10.1021/jacs.9b06299
J. Am. Chem. Soc. 2019, 141, 13212−13221

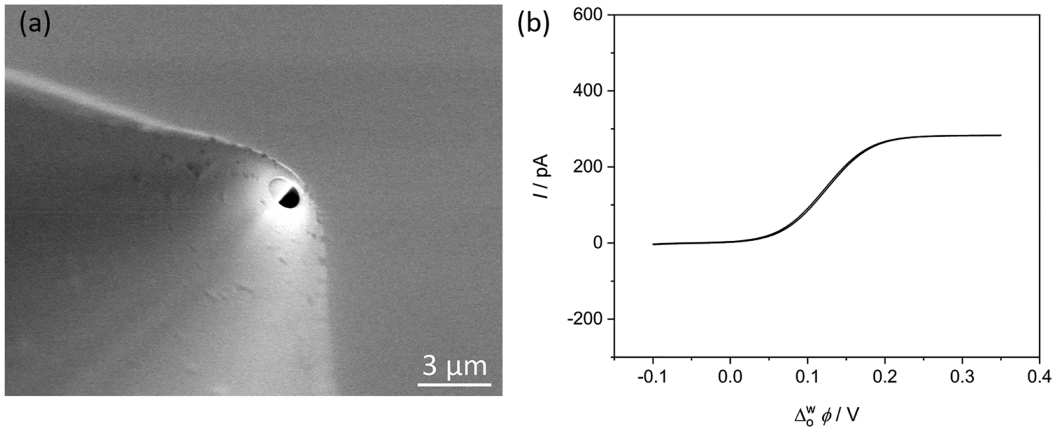

Figure 1. (a) ESEM image of the agar-gel ultramicroelectrode with the agar-gel electrode on the top and pipet underneath. (b) Cyclic voltammogram of the agar-gel ultramicroelectrode with cell S1. Scan rate: 0.02 V s^{-1}.

purchased from Alfa Aesar. Trimethylchlorosilane (TMSCl, ≥99.0%), tetraethylammonium chloride (TEACl, 98%), and tetrabutylammonium iodide (TBAI, 99%) were obtained from Sinopharm Chemical Reagent Company. Bis(triphenylphosphoranylidene)ammonium chloride (BTPPACl, 98.0%) was purchased from Sigma-Aldrich. All these reagents were used as received without purification. Bis(triphenylphosphoranylidene)ammonium tetrakis(pentafluorophenyl)borate (BTPPATPBF$_5$), bis(triphenylphosphoranylidene)ammonium tetrakis(4-chlorophenyl)borate (BTPPATPBCl), and tetraethylammonium tetrakis(4-chlorophenyl)borate (TEATPBCl) were prepared as described previously.[45,46] DCE was distilled before use. All aqueous solutions were prepared with ultrapure water (18.2 MΩ cm).

Fabrication of Agar-Gel Hybrid Ultramicroelectrodes Based on Dual Pipettes. Dual-barrel micropipettes were made from borosilicate glass capillaries (o.d., 1.5 mm, length, 10 cm, Sutter Instrument Co., Novato, CA) based on a P-2000 CO_2-laser-based puller (Sutter Instrument Co.). The pulling program was set as follows: HEAT 550, FIL 4, VEL 30, DEL 135, PULL 20. The dual-barrel micropipettes were examined with an optical microscope (Olympus BX-51, Olympus Co., Japan) to obtain the shape of the tip. To make the outer surface lipophilic, the outer wall and the thin band of the dual-barrel micropipettes were silanized.[47] The tip of the micropipette was put in the vapor of the silanization agent TMSCl solution for 3−5 min, while the argon passed through from the back of the barrels to prevent silanization of the inner walls. Finally, the micropipette was taken out from the vapor and kept in the argon for another 1 min to evaporate residual TMSCl.

Agar-gel microelectrodes were fabricated using the method reported previously, and the amount of agar was a consideration of gelation time.[48] The aqueous solutions were added with agar (2%, w/w) and then heated to about 100 °C until the agar dissolved and the gel became transparent. The hot gel solution was backfilled into one channel of the micropipettes using a small syringe. After cooling to room temperature (22 ± 2 °C), the micropipettes were examined with the optical microscope to ensure that no air bubbles were inside the micropipettes. The radius of the agar-gel microelectrodes was evaluated by the environmental scanning electron microscope (ESEM) and the steady-state voltammograms (Figure 1). Then another channel of the silanized micropipettes was injected with an organic phase, covering the outer surface and making good contact with the gel phase. The details to fabricate water/PVC-gel ultramicroelectrodes are shown in Supporting Information (SI).

Apparatus and Electrochemical Cells. Cyclic voltammetry was performed using a workstation equipped with a bipotentiastat (CHI 760E, Shanghai Chenhua Instruments, Co., China). Mass spectrometry experiments were conducted on an Agilent 6300 Series Ion Trap mass spectrometer (Agilent Technologies, Inc., Santa Clara, CA) in a positive ionization mode. Tandem MS spectra were recorded by collision-induced dissociation (CID) in the ion trap. Data were collected with the following parameters: −500 V end plate offset, 5.0 L/min dry gas, 100 °C dry temperature. A commercial potentiostat (MS-305D, Dongguan Maihao, Ltd., China) was applied as an electrochemical device coupled to mass spectrometry to control the potential of the gel hybrid ultramicroelectrodes. Pulse ionization was achieved with a piezoelectric pistol (Milty Zerostat 3, Goldring, Co., UK). UV absorption spectrometry was recorded with a Hitachi U-4100 spectrophotometer (Hitachi Co., Japan, the quartz cuvette with a path length of 10 mm). An environmental scanning electron microscope (Quanta FEG 250, FEI Co., Hillsboro, OR) was employed to examine the manufactured gel hybrid ultramicroelectrodes, permitting the evaluation of the agar hydrogel electrode without damaging the morphology under low vacuum.

The cells employed in this work are shown in the following:

Cell 1: Ag|AgCl|2% agar + 10 mM LiCl + pH 2.0 (H_2SO_4)‖5 mM BTPPATPBF$_5$ + x mM Fc + y μM CoTPP in DCE|AgTPBF$_5$|Ag.

Cell 2: Ag|AgCl|2% agar + 10 mM LiCl + pH 2.0−4.0 (H_2SO_4), pH 6.8 (without H_2SO_4)‖5 mM BTPPATPBF$_5$ + 5 mM Fc + 50 μM CoTPP in DCE|AgTPBF$_5$|Ag.

Cell 3: Ag|AgCl|10 mM LiCl + pH 1.0−3.0 (H_2SO_4), pH 6.8 (without H_2SO_4)‖10% PVC + 5 mM BTPPATPBF$_5$ + 5 mM Fc + 50 μM CoTPP|AgTPBF$_5$|Ag.

Cell 4: Ag|AgCl|2% agar + 10 mM LiCl + 10 mM TMACl‖50 μM BTPPATPBF$_5$ in DCE|AgTPBF$_5$|Ag.

Cell 5: Ag| AgCl|2% agar + 10 mM LiCl + pH 2.0 (H_2SO_4)‖50 μM BTPPATPBF$_5$ + 5 mM Fc + 0.5 mM CoTPP in DCE|AgTPBF$_5$|Ag.

Cell 6: Ag|AgCl|10 mM LiCl + pH 2.0 (H_2SO_4)‖10% PVC + 5 mM BTPPATPBF$_5$ + 5 mM Fc + 0.5 mM CoTPP|AgTPBF$_5$|Ag.

RESULTS AND DISCUSSION

Characterization of the Gel Hybrid Ultramicroelectrodes and ORR Performance at the Agar-Gel/DCE Interfaces. In our previous investigation, we developed a novel EC-MS technique of hybrid microelectrodes based on dual glass micropipettes (one channel is a carbon micro/nanoelectrode and the other is an empty micro/nanochannel).[38] Combined with a potentisostat, a piezoelectric pistol as pulse ion source, and a mass spectrometer as the detector, the reactions at the carbon/electrolyte interface could be easily studied (similar to the Scheme 1a). In the investigation of a liquid/liquid interface, when the tip of the dual micropipette was silanized and one channel was filled with organic phase and another with aqueous phase, the L/L interface could be formed at the tip of the pipet. Nevertheless, the EC-MS study of oxygen reduction by existence of Fc with CoTPP as the molecular catalyst could only observe the mixture of reactants in both phases and could not obtain the

DOI: 10.1021/jacs.9b06299
J. Am. Chem. Soc. 2019, 141, 13212−13221

intermediates (results not shown here). That is because both phases could be sprayed out by triggering the piezoelectric pistol. To study the interfacial reactions at an L/L interface, we have fabricated two types of new hybrid ultramicroelectrodes: one is a channel filled with agar-gel and the other with organic phases; another hybrid ultramicroelectrode is one channel filled with PVC-gel and the other with aqueous phases. Their characterizations are summarized in SI.

The agar-gel ultramicroelectrodes were characterized by both ESEM and voltammetry of facilitated ion transfer of K^+ by DB18C6 (details shown in S1 of SI). The ESEM image in Figure 1a clearly shows that the agar-gel was filled to the tip of one channel and the other channel was empty. The radius of the ultramicroelectrode was ca. 700 nm. As seen from Figure 1b, the radius of the empty channel was ca. 710 nm, which was consistent with that obtained by the ESEM image.

The EC study of the ORR by Fc with CoTPP as the molecular catalyst was carried out at the agar-gel/DCE interface using cyclic voltammetry. Figure 2 displays the cyclic voltammograms obtained under different experimental conditions using cell 1. In Figure 2a, without the presence of Fc and CoTPP, the voltammetric response (black curve) showed the potential window (it was very similar to the classical potential window obtained at the W/DCE interface, see Figure S4 in SI). At positive potential, the potential window was limited by the transfer of H^+/Li^+ from the aqueous to the organic phase or $TPBF_5^-$ from the organic to the aqueous phase, and the negative potential window was controlled by the transfer of SO_4^{2-}, Cl^-, or $BTPPA^+$. Compared to the blank response, the presence of CoTPP showed no obvious changes (red curve), indicating that no obvious adsorption of CoTPP at the interface could be observed. As shown in Figure 2b, when Fc and CoTPP were both in the solution, the voltammetric response (blue curve) showed a negative current at −0.15 to 0 V (half-wave potential, $E_{1/2}$ = −0.07 V), consistent with ion transfer (IT) of ferricenium cations (Fc^+) from the organic phase to the aqueous phase. Moreover, a positive current at 0 to 0.15 V ($E_{1/2}$ = 0.07 V) was acquired, attributed to an interfacial electron transfer reaction between Fc and O_2, which was analogous to the previous study of the interfacial redox reaction between decamethylferrocene (DCMFc) in DCE and oxygen in the aqueous phase.[49] In particular, the transfer of Fc^+ from aqueous phase to DCE, or oxygen intermediate, e.g., superoxide anion, from DCE to aqueous phase, should be excluded because the concentrations in the corresponding phases were too low to produce the positive signal shown in Figure 2b.[49] Note that in the presence of only Fc in DCE, small waves were observed (black curve), showing that the Fc was slowly oxidized on its own during the measurement time scale. In the control experiment under anaerobic conditions, the current signals disappeared (red curve), confirming that the aforementioned negative current and positive current are related to the O_2 reduction. Clearly, the presence of Fc, CoTPP, and O_2 and the H^+ transfer from agar-gel to organic phase are necessary to obtain these coupled signals. These results are in good agreement with that in the proposed mechanism in Scheme 1b. Here the only function of the aqueous (agar-gel phase) phase is to provide protons to initiate these reactions. In addition, the agar-gel/DCE interface is also verified to be very similar to that of a W/DCE interface.

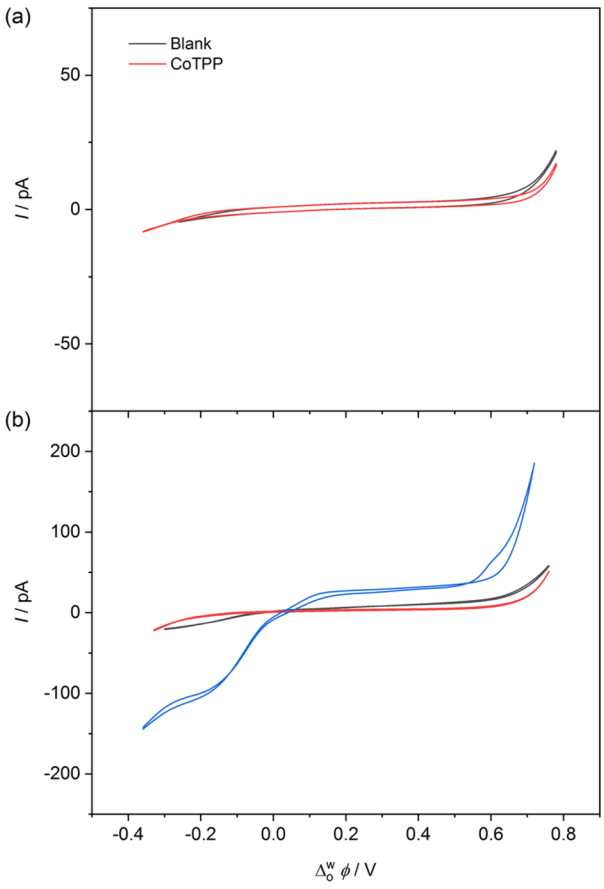

Figure 2. (a) Cyclic voltammograms with cell 1 (x = 0, y = 50) in the absence (black curve) and presence (red curve) of CoTPP conducted with agar-gel/DCE ultramicroelectrodes. (b) Cyclic voltammograms with cell 1 in the presence of only Fc (black curve, x = 5, y = 0) and both Fc and CoTPP (blue curve, x = 5, y = 50). The red curve was conducted under anaerobic conditions, but the others were the same as the blue curve. Scan rate: 0.05 V s^{-1}.

The two possible pathways involved in this work could be expressed as[44]

$$2Fc_{(DCE)} + O_{2(DCE)} + 2H^+_{(w)} \xrightarrow{CoTPP} 2Fc^+_{(DCE)} + H_2O_{2(w)} \quad (1)$$

and/or

$$4Fc_{(DCE)} + O_{2(DCE)} + 4H^+_{(w)} \xrightarrow{CoTPP} 4Fc^+_{(DCE)} + 2H_2O_{(w)} \quad (2)$$

They represent a two-electron/two-proton oxygen reduction pathway and a four-electron/four-proton oxygen reduction pathway, respectively. By variation of the pH of the agar phase, the influence of hydrogen ions on the PCET reaction was observed. The pH was adjusted from 2.0 to 4.0 using the electrochemical cell 2. The Nernst equations for the possible PCET reactions shown in eqs 1 and 2 are listed in the following:[44,50]

$$\Delta^w_o\phi_{2et} = \Delta^w_o\phi^0_{2et} + \frac{RT\ln 10}{F}\text{pH} + \frac{RT}{2F}\ln\left[\left(\frac{a^o_{Fc^+}}{a^o_{Fc}}\right)^2\left(\frac{p^0}{f_{O_2}}\right)a^w_{H_2O_2}\right] \quad (3)$$

DOI: 10.1021/jacs.9b06299
J. Am. Chem. Soc. 2019, 141, 13212−13221

$$\Delta_o^w\phi_{4et} = \Delta_o^w\phi_{4et}^0 + \frac{RT\ \ln 10}{F}\mathrm{pH} + \frac{RT}{4F}\ln\left[\left(\frac{a_{Fc^+}^o}{a_{Fc}^o}\right)^4\left(\frac{p^0}{f_{O_2}}\right)(a_{H_2O}^w)^2\right] \quad (4)$$

where a_i^o is the activity of species i in the organic phase, p^0 is the standard pressure, f_{O2} represents the fugacity of oxygen, and $\Delta_o^w\phi_{2et}^0$ and $\Delta_o^w\phi_{4et}^0$ are the standard potential for the two-electron or four-electron interfacial PCET mechanisms, respectively.

Figure 3 shows a negative wave at about −0.15 to 0 V ($E_{1/2}$ = −0.07 V) ascribed to transfer of Fc^+ across agar-gel/DCE

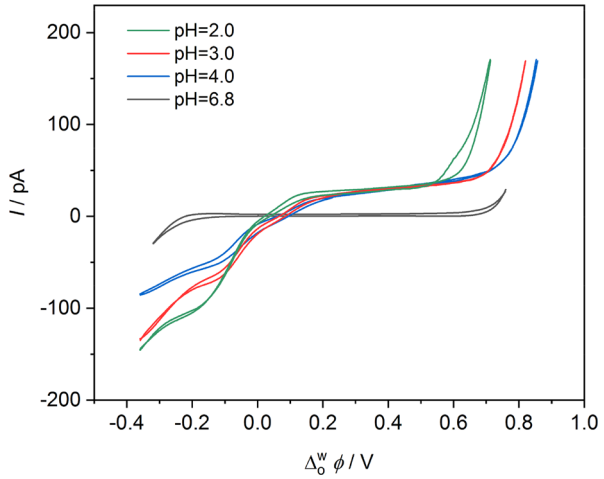

Figure 3. Cyclic voltammograms with cell 2 at pH 2.0 (green), pH 3.0 (red), pH 4.0 (blue), and pH 6.8 (black) conducted with agar-gel/DCE ultramicroelectrodes. Scan rate: 0.05 V s^{-1}.

interface and a positive current at 0 to 0.15 V ($E_{1/2}$ = 0.07 V) assigned to the electron transfer reaction between Fc in DCE and O_2 in aqueous phase. With the concentration of H^+ in the aqueous phase increasing, more H^+ transferred to the interface and then more Fc^+ was produced during the PCET processes, making the negative waves increase successively. The positive currents were not influenced by the pH, which might result from the excess protons in the aqueous phase. The agar would be degraded at low pH; thus, the pH was set from 2.0 to 4.0. By changing the pH from 2.0 (~10^{-2} M) to 3.0 (~10^{-3} M), the current signal moved to the right about 60 mV/pH, as predicted by eqs 3 and 4. The potential windows were controlled by Li^+ and H^+ at the positive potential. With the decrease in concentration of H^+, Li^+ might become the limiting factor, leading to less change in the positive potential window from pH 3.0 to pH 4.0. In contrast, in the absence of additional acid in the aqueous phase, no significant signal was observed, proving the necessity of the presence of H^+ in the ORR. The results of the pH dependence experiments indicate that the current waves shift with pH at positive potentials. The CV measurements show that the electrochemical responses of agar-gel/DCE micropipettes are consistent with those obtained at the water/DCE interface,[44,51] proving that the PCET reactions at the agar-gel/DCE interface are by nature very similar to those at a water/DCE phase interface.

ORR Behaviors at the Water/PVC-Gel Interfaces. The CV measurements were also conducted at the water/PVC-gel ultramicroelectrodes using electrochemical cell 3 for the ORR at the water/PVC-gel interfaces (Figure 4). Compared with

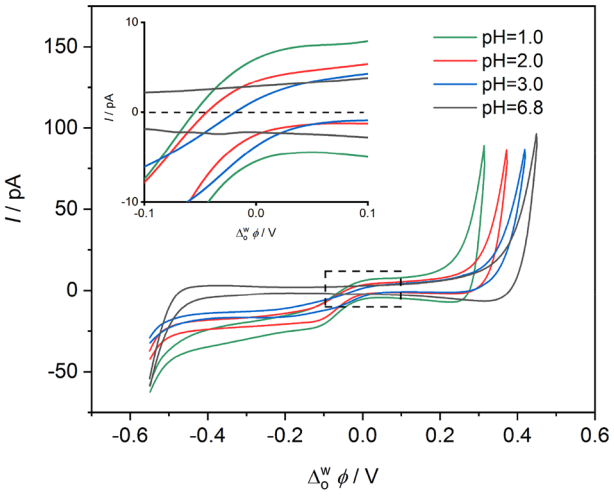

Figure 4. Cyclic voltammograms with cell 3 at pH 1.0 (green), pH 2.0 (red), pH 3.0 (blue), and pH 6.8 (black) conducted with water/PVC-gel ultramicroelectrodes. Scan rate: 0.05 V s^{-1}.

the agar-gel ultramicroelectrodes with poor performance at low pH, the water/PVC-gel ultramicroelectrodes could be used at low pH. The cyclic voltammograms showed a negative current at −0.1 to 0 V ($E_{1/2}$ = −0.06 V) corresponding with Fc^+ from the organic phase to the aqueous phase. With the pH shifting from 3.0 to 1.0, more Fc^+ was generated and the negative currents increased accordingly. The current signals shifted with pH around 60 mV/pH at the positive potential, consistent with eqs 3 and 4. When no additional acid was put into the aqueous phase, the transfer signal of Fc^+ was absent, which was the same with the result at the agar-gel/DCE interface. As shown in the inset, the positive currents due to the reaction between Fc and O_2 observed in agar-gel/DCE interface were rather small here, which might be an influence of the slow diffusion coefficient of the Fc in the PVC gel, decreasing the chance of reaction between Fc in the PVC-gel and O_2 in the aqueous phase. The CV measurements indicate that the electrochemical responses of water/PVC-gel interfaces are also in accord with the results at the water/DCE interface.

EC-MS Studies of the Interfacial ORR at the Gel/Electrolyte Interfaces. In the EC-MS measurements, as a proof-of-concept application, a simple ion (tetramethylammonium, TMA^+) transfer at the agar-gel/organic interface was conducted using cell 4 (EC result is shown in Figure S8, and the setup is shown in Figure S9). First, to verify the stability of the agar-gel ultramicroelectrodes, an MS test of the agar-gel micropipettes without organic phase was carried out. In this case, the agar-gel micropipette was equivalent to the mass spectrometer spray emitter. The results of the mass spectrometry revealed that in the absence of TMA^+, only the background signal of air was detected (Figure S10), indicating that the aqueous phase could be successfully immobilized by addition of agar and would not be delivered into the mass spectrometer during the ionization process. Then the simple ion transfer of TMA^+ at the agar-gel/DCE interface was performed with another channel of the micropipette filled with DCE phase. When the potential was turned off, as seen in Figure 5, TMA^+ m/z 74 and the background of the organic residue, such as m/z 86 single peak, were observed. Note that

DOI: 10.1021/jacs.9b06299
J. Am. Chem. Soc. 2019, 141, 13212−13221

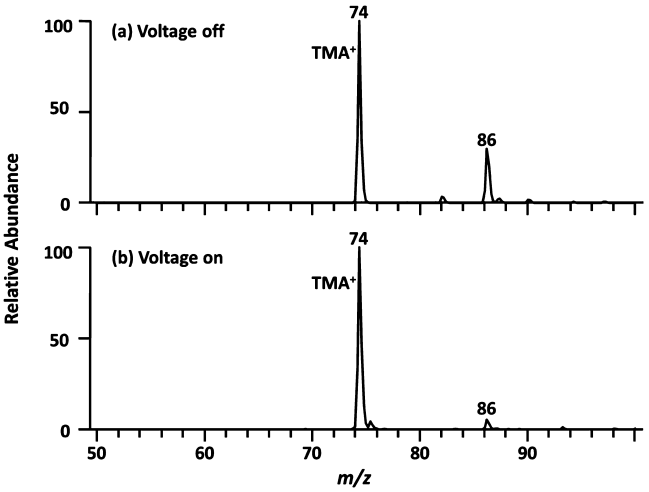

Figure 5. (a) A representative mass spectrum when the voltage was off. (b) A representative mass spectrum when 0.5 V was applied using cell 4, for detection of TMA^+.

the detection of TMA^+ resulted from dispersal in organic solution. The intensity of the m/z 74 ion to the m/z 86 ion (I_{74}/I_{86}) was 3.4. When the potential was set as 0.5 V, the TMA^+ would transfer from agar-gel phase to the organic phase, significantly increasing the TMA^+ signal compared with the compressed signal of the background at m/z 86 (I_{74}/I_{86} = 19.2). According to the previous work,[38] when another channel of agar-gel micropipette was filled with the organic phase, the agar-gel/organic phase interface was quickly formed. Combined with the pulse ionization, the reactants, products, and intermediates at the interfacial layer were quickly going with the organic solution to the MS detector. The results of simple ion transfer at the agar-gel/organic interfaces confirm that the EC-MS setup is capable of detecting the products and possible intermediates at the interfacial layer.

Using the EC-MS setup illustrated in the Scheme 1, the ORR electrocatalyzed by CoTPP was monitored using electrochemical cell 5 as shown in Figure 6. When the voltage applied at the agar-gel/DCE interfaces was 0.0 V, only the $CoTPP^+$ m/z 671 was produced (Figure 6a). The detection of $CoTPP^+$ might be due to the loss of one electron of the neutral CoTPP compound during the ionization. Figure 6b illustrates that when the voltage was set at −0.7 V, the proton would proceed to the organic phase, triggering a series of reactions occurring at the interface. The signals of m/z 688 and m/z 703 with similar isotopic distributions of CoTPP (inset) were detected simultaneously by mass spectrometry, which indicated that the peaks were closely related to the CoTPP complexes.

To further help with the interpretation of the peaks, the ions were fragmented by collision-induced dissociation. Figure 6c shows a predominant fragment ion at m/z 671. Moreover, an ion peak at m/z 611 was also detected, which coincided with the loss of a phenyl group from parent ion m/z 688, further confirming that the peak at m/z 688 corresponded to $(Co{-}OH)TPP^+$. Utilizing the same methodology, the CID analysis of m/z 703 was carried out (Figure 6d). The presence of a fragment ion at m/z 671 indicated the formation of $(Co{-}O_2)TPP^+$. It should be noted that the detection of cations of $(Co{-}OH)TPP^+$ and $(Co{-}O_2)TPP^+$ should result from the ionization of the neutral $(Co{-}OH)TPP$ and $(Co{-}O_2)TPP$ compounds.

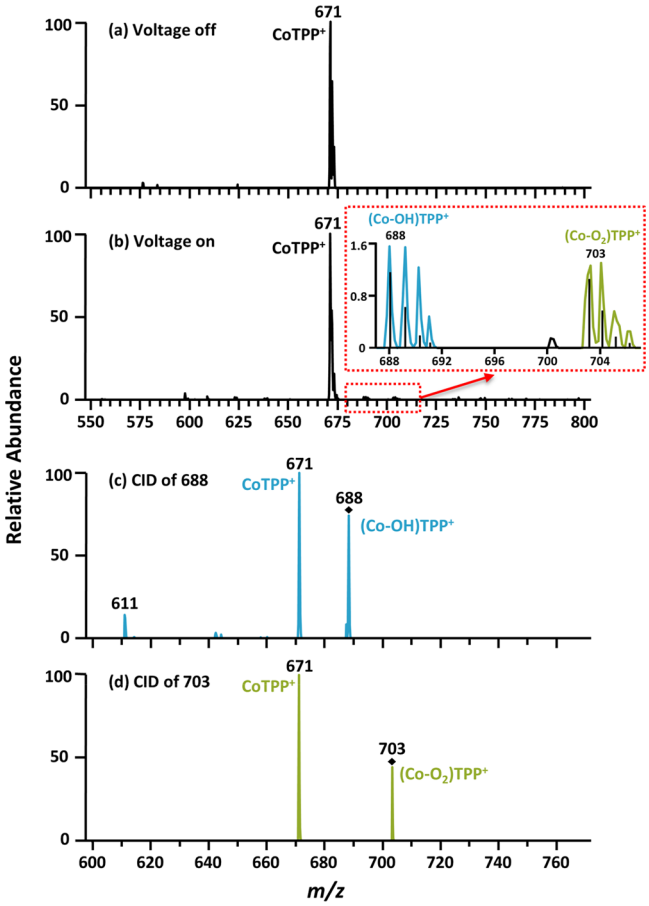

Figure 6. (a) Mass spectrum when the voltage was off. (b) Mass spectrum when 0.7 V was applied using cell 5, detection of the CoTPP complex intermediates. CID spectra of m/z 688 (c) and m/z 703 (d). The inset is the isotopic distributions of $(Co{-}OH)TPP$ (blue), $(Co{-}O_2)TPP$ (green), and CoTPP (black).

EC-MS studies of the ORR at water/PVC-gel interfaces were also conducted using cell 6 (Figure 7). In this case, the aqueous phase was sprayed out with the intermediates and products in the interfacial reactions. When the potential was off, only $BTPPA^+$ m/z at 538 and background signals of the

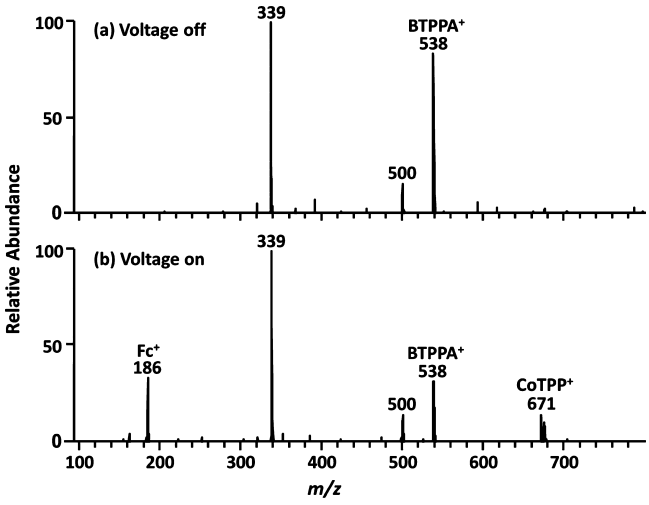

Figure 7. (a) Mass spectrum when the voltage was off. (b) Mass spectrum when 0.7 V was applied using cell 6.

DOI: 10.1021/jacs.9b06299
J. Am. Chem. Soc. 2019, 141, 13212−13221

water residue (m/z 339 and m/z 500) were detected. Applying a potential of 0.7 V to the L/L interface resulted in a decline of the $BTPPA^+$ signal, which was suppressed by the positive potential employed at the aqueous phase. Compared to the signals obtained without externally applied potential, Fc^+ m/z at 186 and $CoTPP^+$ m/z at 671 were detected with 0.7 V applied potential, proving the detection of some of the products and intermediates of the interfacial PCET. However, the complexes of CoTPP with O_2 and OH could not be observed. The reasons might be that the concentration of O_2 trapped inside the gel of the organic phase was rather low, the very slow diffusion rate of existent O_2 within the organic gel, and the distribution of formed CoTPP complexes in the PVC-gel into the aqueous phase or interface was very rare.

Mechanism of the Interfacial ORR. The ORR catalyzed by metalloporphyrins has been widely explored both in the homogeneous phase[52−55] and in the heterogeneous phase, e.g., the L/L interfaces.[44] Herein the performance of CoTPP catalyst at the L/L interfaces was revealed based on the aforementioned experimental results. Clearly, the presence of product Fc^+ could be revealed by the EC experiments. The EC-MS experiments based on the W/PVC-gel hybrid ultramicroelectrodes provided direct evidence for the products Fc^+ and intermediates $CoTPP^+$. The experiments based on the agar-gel/O interface have shown the presence of intermediates $(Co-O_2)TPP$ and (Co−OH)TPP. A mechanism for the ORR catalyzed by CoTPP was put forward as follows, based on the experimental results and previous reports.[56] During the ORR, O_2 inserts into Co^{II}-TPP, generating a superoxide intermediate:[57]

$$Co^{II}TPP_{(DCE)} + O_{2(DCE)} \rightarrow (Co^{II}-O_2)TPP/(Co^{III}-O_2^-)TPP_{(DCE)} \quad (5)$$

With one electron donor Fc and one proton reacting with electron acceptor $(Co^{II}-O_2)TPP$ or $(Co^{III}-O_2^-)TPP$, PCET reaction would take place to produce hydroperoxo adduct:

$$(Co^{III}-O_2^-)TPP_{(DCE)} + Fc_{(DCE)} + H^+_{(w)} \rightarrow (Co^{III}-OOH)TPP_{(DCE)} + Fc^+_{(DCE)} \quad (6)$$

After that, $(Co^{III}-OOH)TPP$ might undergo O−O bond cleavage to generate $(Co^{IV}=O)TPP$ and lead to the formation of H_2O:

$$(Co^{III}-OOH)TPP_{(DCE)} + Fc_{(DCE)} + H^+_{(w)} \rightarrow (Co^{IV}=O)TPP_{(DCE)} + Fc^+_{(DCE)} + H_2O_{(w)} \quad (7)$$

Subsequently, the $(Co^{IV}=O)TPP$ would capture one electron and one proton to form OH on a Co atom:

$$(Co^{IV}=O)TPP_{(DCE)} + Fc_{(DCE)} + H^+_{(w)} \rightarrow (Co^{III}-OH)TPP_{(DCE)} + Fc^+_{(DCE)} \quad (8)$$

Finally, the $(Co^{III}-OH)TPP$ intermediate would obtain one electron and one proton to produce H_2O:

$$(Co^{III}-OH)TPP_{(DCE)} + Fc_{(DCE)} + H^+_{(w)} \rightarrow Co^{II}TPP_{(DCE)} + Fc^+_{(DCE)} + H_2O_{(w)} \quad (9)$$

Alternatively, $(Co^{III}-OOH)TPP$ might be involved to produce H_2O_2 as shown in the following step:

$$(Co^{III}-OOH)TPP_{(DCE)} + H^+_{(w)} \rightarrow Co^{III}TPP^+_{(DCE)} + H_2O_{2(w)} \quad (10)$$

and $Co^{II}TPP$ was regenerated by the following reaction:

$$Co^{III}TPP^+_{(DCE)} + Fc_{(DCE)} \rightarrow Co^{II}TPP_{(DCE)} + Fc^+_{(DCE)} \quad (11)$$

As demonstrated above, the (Co−OOH)TPP and (Co=O)TPP intermediates were not detected, which might be a reason that the two intermediates were quite unstable and spontaneously decayed in the subsequent reactions or low equilibrium concentrations in the solution or in the gas phase. The (Co−OH)TPP intermediate was the third step (three electrons and three protons were involved) in the four-electron/four-proton oxygen reduction pathway to produce H_2O, which was absent in the two-electron reduction. Thus, the detection of (Co−OH)TPP by EC-MS proved the presence of the four-electron reduction pathway. Moreover, the biphasic reactions controlled by chemical polarization (common ions in both phases) were performed with shaking both aqueous and DCE phases in a flask and monitoring the products by UV−vis spectroscopy (Figure S11). The experimental results demonstrated that the number of transferred electrons per molecular oxygen reduction was 3.9 and the selectivity of four-electron reduction of O_2 was more than 94%, further confirming the high selectivity to produce H_2O. According to EC-MS and UV−vis study, two-electron and four-electron pathways both existed in the ORR catalyzed by CoTPP and the latter was the main pathway. To our knowledge, the majority of the previous studies suggested that the monomeric cobalt porphyrins catalyzed a two-electron reduction of O_2 to produce H_2O_2 in the homogeneous phase.[58,59] Nevertheless, Anson et al. have reported that CoTPP catalyzed the four-electron reduction of O_2 to produce H_2O at the L/L interface.[60] In addition, surprisingly low H_2O_2 yields in the oxygen reduction with CoTPP as the catalyst in the two-phase reaction was also observed.[61] In this work, we attribute the main four-electron pathway catalyzed by CoTPP to the following reason. Naturally, the two-electron and four-electron pathways were in parallel at comparable rates. H^+ and CoTPP catalyst were in the separated phases; in this case, the mass transport of proton across the W/DCE interface might become the rate-limiting step of the ORR.[56] A low equilibrium concentration of protons at the interface makes step 10 slower; thus, O_2 had a longer time to coordinate with the cobalt center to accept additional electrons to produce H_2O. This proposal was confirmed by the homogeneous oxygen reduction reaction (S6 in SI), which proceeded mainly through the two-electron reduction pathway. Therefore, in contrast to the homogeneous oxygen reduction reaction favoring the two-electron pathway, the heterogeneous oxygen reduction reaction with monomeric cobalt-based catalysts is dominated by the four-electron pathway.

Theoretical Calculation. Calculation was carried out to investigate the possibility of the intermediates and the four-electron oxygen reduction pathway. More details of the calculation are shown in S7 of SI. The highest occupied molecular orbital (HOMO) and lowest unoccupied molecular orbital (LUMO) of CoTPP are depicted in Figure 8a and 8b.

DOI: 10.1021/jacs.9b06299
J. Am. Chem. Soc. 2019, 141, 13212−13221

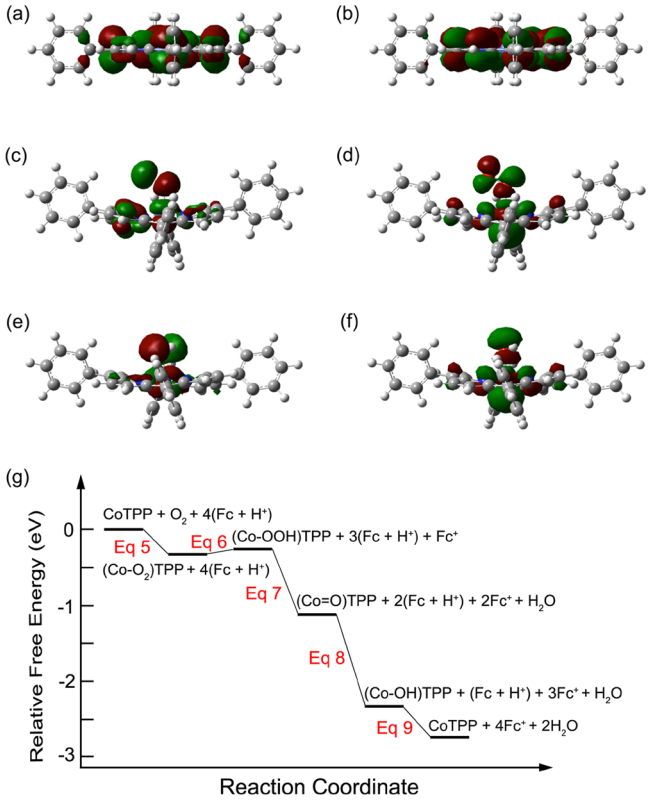

Figure 8. (a, c, e) HOMO of CoTPP, (Co−O_2)TPP, and (Co−OH)TPP. (b, d, f) LUMO of CoTPP, (Co−O_2)TPP, and (Co−OH)TPP. (g) Relative free energy (considering solvation effect) profile of the four-electron oxygen reduction pathway in eqs 5−9, which are −0.323, 0.054, −0.859, −1.237, and −0.369 eV, respectively.

In contrast, the molecular orbitals (MOs) of the CoTPP complex with O_2 (Figure 8c,d) and that with OH (Figure 8e,f) absorption were also investigated. When CoTPP was combined with O_2 or OH, the significant change of the structure indicated the strong interaction between them. The Co−O bond lengths of (Co−O_2)TPP, (Co−OOH)TPP, (Co═O)TPP, and (Co−OH)TPP were suggested to be 1.90, 1.87, 1.73, and 1.86 Å, respectively, as shown in Figure S13. In addition, the relative Gibbs free energy (G) of the four-electron pathway at 298 K and 1 atm pressure in eqs 5−9 was demonstrated in Figure 8g. The calculation suggested that the change of the Gibbs free energy (ΔG) of each step was negative, except that of eq 6 was slightly positive. This hinted that all the processes were energy-favorable and that the proposed four-electron reduction mechanism was reasonable in terms of thermodynamics. More investigation on dynamics will be interesting in the future. These simulation results supported that it was possible to form the (Co−O_2)TPP and (Co−OH)TPP complexes in the four-electron pathway.

CONCLUSIONS

In summary, we fabricated agar-gel/W and PVC-gel/O hybrid ultramicropipettes to function as the liquid/liquid interfaces and microelectrochemical cells. Combined with a mass spectrometer as the detector, a novel EC-MS hyphenated technique was established to provide real time and online information on the interfacial electrochemical reactions. The electrochemical studies were performed to verify the responses of the agar-gel/DCE interface and water/PVC-gel interface and were very similar to that of a classical W/DCE interface. Using gel hybrid ultramicroelectrodes, the mechanism of the interfacial ORR by Fc with CoTPP as the molecular catalyst was investigated online by EC-MS. The key (Co−O_2)TPP and (Co−OH)TPP intermediates of the interfacial reaction were determined in this work for the first time. Theoretical calculation was performed and further supported the rationality of the (Co−O_2)TPP and (Co−OH)TPP intermediates. Along with the biphasic reactions, the ORR catalyzed by CoTPP at the L/L interface was concluded to proceed preferentially via a four-electron pathway to produce H_2O. This method is general and might open a wide applicability for the mechanistic study of reactions at L/L interfaces or other soft interfaces.

ASSOCIATED CONTENT

Supporting Information

The Supporting Information is available free of charge on the ACS Publications Web site. (PDF). The Supporting Information is available free of charge on the ACS Publications website at DOI: 10.1021/jacs.9b06299.

Experimental details and electrochemistry data of the gel hybrid ultramicroelectrodes, photograph of the EC-MS setup, biphasic reactions and homogeneous reactions by UV−vis, and details of the theoretical analysis (PDF)

AUTHOR INFORMATION

Corresponding Author

*yhshao@pku.edu.cn

ORCID

Jian Liu: 0000-0002-2906-5858

Yuanhua Shao: 0000-0003-3922-6229

Author Contributions

The manuscript was written through contributions of all authors. All authors have given approval to the final version of the manuscript.

Notes

The authors declare no competing financial interest.

ACKNOWLEDGMENTS

The financial support for this work from the National Key Research and Development Program of China (no. 2016YFA0201300) and the National Natural Science Foundation of China (21575006 and 21335001) is gratefully acknowledged.

REFERENCES

(1) Hammes-Schiffer, S.; Stuchebrukhov, A. A. Theory of Coupled Electron and Proton Transfer Reactions. *Chem. Rev.* **2010**, *110*, 6939−6960.

(2) Qiu, G.; Knowles, R. R. Rate-Driving Force Relationships in the Multisite Proton-Coupled Electron Transfer Activation of Ketones. *J. Am. Chem. Soc.* **2019**, *141*, 2721−2730.

(3) Costentin, C.; Robert, M.; Saveant, J. M. Update 1 of: Electrochemical Approach to the Mechanistic Study of Proton-Coupled Electron Transfer. *Chem. Rev.* **2010**, *110*, Pr1−Pr40.

(4) Kuss-Petermann, M.; Orazietti, M.; Neuburger, M.; Hamm, P.; Wenger, O. S. Intramolecular Light-Driven Accumulation of Reduction Equivalents by Proton-Coupled Electron Transfer. *J. Am. Chem. Soc.* **2017**, *139*, 5225−5232.

DOI: 10.1021/jacs.9b06299
J. Am. Chem. Soc. 2019, 141, 13212−13221

(5) Odella, E.; Mora, S. J.; Wadsworth, B. L.; Huynh, M. T.; Goings, J. J.; Liddell, P. A.; Groy, T. L.; Gervaldo, M.; Sereno, L. E.; Gust, D.; Moore, T. A.; Moore, G. F.; Hammes-Schiffer, S.; Moore, A. L. Controlling Proton-Coupled Electron Transfer in Bioinspired Artificial Photosynthetic Relays. *J. Am. Chem. Soc.* **2018**, *140*, 15450−15460.
(6) Adam, S. M.; Wijeratne, G. B.; Rogler, P. J.; Diaz, D. E.; Quist, D. A.; Liu, J. J.; Karlin, K. D. Synthetic Fe/Cu Complexes: Toward Understanding Heme-Copper Oxidase Structure and Function. *Chem. Rev.* **2018**, *118*, 10840−11022.
(7) Belevich, I.; Verkhovsky, M. I.; Wikstrom, M. Proton-coupled electron transfer drives the proton pump of cytochrome c oxidase. *Nature* **2006**, *440*, 829−832.
(8) Magnuson, A.; Anderlund, M.; Johansson, O.; Lindblad, P.; Lomoth, R.; Polivka, T.; Ott, S.; Stensjo, K.; Styring, S.; Sundstrom, V.; Hammarstrom, L. Biomimetic and Microbial Approaches to Solar Fuel Generation. *Acc. Chem. Res.* **2009**, *42*, 1899−1909.
(9) Esswein, A. J.; Nocera, D. G. Hydrogen production by molecular photocatalysis. *Chem. Rev.* **2007**, *107*, 4022−4047.
(10) Siewert, I. Proton-Coupled Electron Transfer Reactions Catalysed by 3d Metal Complexes. *Chem. - Eur. J.* **2015**, *21*, 15078−15091.
(11) Meyer, T. J.; Huynh, M. H. V.; Thorp, H. H. The possible role of proton-coupled electron transfer (PCET) in water oxidation by photosystem II. *Angew. Chem., Int. Ed.* **2007**, *46*, 5284−5304.
(12) Dau, H.; Zaharieva, I. Principles, Efficiency, and Blueprint Character of Solar-Energy Conversion in Photosynthetic Water Oxidation. *Acc. Chem. Res.* **2009**, *42*, 1861−1870.
(13) Sirohiwal, A.; Neese, F.; Pantazis, D. A. Microsolvation of the Redox-Active Tyrosine-D in Photosystem II: Correlation of Energetics with EPR Spectroscopy and Oxidation-Induced Proton Transfer. *J. Am. Chem. Soc.* **2019**, *141*, 3217−3231.
(14) Olaya, A. J.; Schaming, D.; Brevet, P. F.; Nagatani, H.; Zimmermann, T.; Vanicek, J.; Xu, H. J.; Gros, C. P.; Barbe, J. M.; Girault, H. H. Self-Assembled Molecular Rafts at Liquid vertical bar Liquid Interfaces for Four-Electron Oxygen Reduction. *J. Am. Chem. Soc.* **2012**, *134*, 498−506.
(15) Wang, L.; Van Voorhis, T. Direct-Coupling O_2 Bond Forming a Pathway in Cobalt Oxide Water Oxidation Catalysts. *J. Phys. Chem. Lett.* **2011**, *2*, 2200−2204.
(16) Bozoglian, F.; Romain, S.; Ertem, M. Z.; Todorova, T. K.; Sens, C.; Mola, J.; Rodriguez, M.; Romero, I.; Benet-Buchholz, J.; Fontrodona, X.; Cramer, C. J.; Gagliardi, L.; Llobet, A. The Ru-Hbpp Water Oxidation Catalyst. *J. Am. Chem. Soc.* **2009**, *131*, 15176−15187.
(17) Liu, S.; Li, Q.; Shao, Y. Electrochemistry at micro- and nanoscopic liquid/liquid interfaces. *Chem. Soc. Rev.* **2011**, *40*, 2236−2253.
(18) Benjamin, I. Mechanism and Dynamics of Ion Transfer across a Liquid-Liquid Interface. *Science* **1993**, *261*, 1558−1560.
(19) Reymond, F.; Fermin, D.; Lee, H. J.; Girault, H. H. Electrochemistry at liquid/liquid interfaces: methodology and potential applications. *Electrochim. Acta* **2000**, *45*, 2647−2662.
(20) Zhang, S.; Li, M.; Su, B.; Shao, Y. Fabrication and Use of Nanopipettes in Chemical Analysis. *Annu. Rev. Anal. Chem.* **2018**, *11*, 265−286.
(21) Shao, Y.; Mirkin, M. V. Fast kinetic measurements with nanometer-sized pipets. Transfer of potassium ion from water into dichloroethane facilitated by dibenzo-18-crown-6. *J. Am. Chem. Soc.* **1997**, *119*, 8103−8104.
(22) Scanlon, M. D.; Herzog, G.; Arrigan, D. W. M. Electrochemical detection of oligopeptides at silicon-fabricated micro-liquid vertical bar liquid interfaces. *Anal. Chem.* **2008**, *80*, 5743−5749.
(23) Yuan, Y.; Amemiya, S. Facilitated protamine transfer at polarized water/1,2-dichloroethane interfaces studied by cyclic voltammetry and chronoamperometry at micropipet electrodes. *Anal. Chem.* **2004**, *76*, 6877−6886.
(24) Zhan, D.; Mao, S.; Zhao, Q.; Chen, Z.; Hu, H.; Jing, P.; Zhang, M.; Zhu, Z.; Shao, Y. Electrochemical investigation of dopamine at the water/1,2-dichloroethane interface. *Anal. Chem.* **2004**, *76*, 4128−4136.
(25) Peljo, P.; Qiao, L.; Murtomaki, L.; Johans, C.; Girault, H. H.; Kontturi, K. Electrochemically Controlled Proton-Transfer-Catalyzed Reactions at Liquid-Liquid Interfaces: Nucleophilic Substitution on Ferrocene Methanol. *ChemPhysChem* **2013**, *14*, 311−314.
(26) Oue, M.; Kimura, K.; Shono, T. Liquid-Liquid-Extraction of Silver Ion with Benzothiacrown Ether Derivatives. *Anal. Chim. Acta* **1987**, *194*, 293−298.
(27) Lam, H. T.; Pereira, C. M.; Roussel, C.; Carrupt, P. A.; Girault, H. H. Immobilized pH gradient gel cell to study the pH dependence of drug lipophilicity. *Anal. Chem.* **2006**, *78*, 1503−1508.
(28) Zhang, M.; Sun, P.; Chen, Y.; Li, F.; Gao, Z.; Shao, Y. Studies of effect of phase volume ratio on transfer of ionizable species across the water/1,2-dichloroethane interface by a three-electrode setup. *Anal. Chem.* **2003**, *75*, 4341−4345.
(29) Wang, D.; Zhang, M.; Buhlmann, P.; Que, L. Redox Potential and C-H Bond Cleaving Properties of a Nonheme Fe-IV═O Complex in Aqueous Solution. *J. Am. Chem. Soc.* **2010**, *132*, 7638−7644.
(30) Rudolph, M.; Reddy, D. P.; Feldberg, S. W. A Simulator for Cyclic Voltammetric Responses. *Anal. Chem.* **1994**, *66*, A589−A600.
(31) Guo, S.; Mariotti, A. W. A.; Schlipf, C.; Bond, A. M.; Wedd, A. G. Investigation of the pronounced medium effects observed in the voltammetry of the highly charged lacunary anions $[\alpha\text{-SiW}_{11}O_{39}]^{8-}$ and $[\alpha\text{-PW}_{11}O_{39}]^{7-}$. *Inorg. Chem.* **2006**, *45*, 8563−8574.
(32) Parthasarathy, M.; Gopinath, C. S.; Vijayamohanan. Autoreduction of cyanoferrate(III) ions in a polymer electrolyte membrane: All solid state electrochemical and spectroscopic investigations. *Chem. Mater.* **2006**, *18*, 5244−5252.
(33) Baitalik, S.; Dutta, S.; Biswas, P.; Florke, U.; Bothe, E.; Nag, K. Structural, Spectroscopic, and Proton-Coupled Electron-transfer Behavior of Pyrazolyl-3,5-bis(benzimidazole)-Bridged Homo- and Heterochiral $Ru^{II}Ru^{II}$, $Os^{II}Os^{II}$, and $Os^{II}Ru^{II}$ 2,2′-Bipyridine Complexes. *Eur. J. Inorg. Chem.* **2010**, *2010*, 570−588.
(34) Liu, P.; Lu, M.; Zheng, Q.; Zhang, Y.; Dewald, H. D.; Chen, H. Recent advances of electrochemical mass spectrometry. *Analyst* **2013**, *138*, 5519−5539.
(35) Bruckenstein, S.; Rao Gadde, R. Use of a Porous Electrode for in-Situ Mass Spectrometric Determination of Volatile Electrode Reaction Products. *J. Am. Chem. Soc.* **1971**, *93*, 793−794.
(36) Brown, T. A.; Chen, H.; Zare, R. N. Identification of Fleeting Electrochemical Reaction Intermediates Using Desorption Electrospray Ionization Mass Spectrometry. *J. Am. Chem. Soc.* **2015**, *137*, 7274−7277.
(37) Brown, T. A.; Chen, H.; Zare, R. N. Detection of the Short-Lived Radical Cation Intermediate in the Electrooxidation of N,N-Dimethylaniline by Mass Spectrometry. *Angew. Chem., Int. Ed.* **2015**, *54*, 11183−11185.
(38) Qiu, R.; Zhang, X.; Luo, H.; Shao, Y. Mass spectrometric snapshots for electrochemical reactions. *Chem. Sci.* **2016**, *7*, 6684−6688.
(39) Prudent, M.; Mendez, M. A.; Jana, D. F.; Corminboeuf, C.; Girault, H. H. Formation and study of single metal ion-phospholipid complexes in biphasic electrospray ionization mass spectrometry. *Metallomics* **2010**, *2*, 400−406.
(40) Stockmann, T. J.; Lu, Y.; Zhang, J.; Girault, H. H.; Ding, Z. F. Interfacial Complexation Reactions of Sr^{2+} with Octyl(phenyl)-N,N-diisobutylcarbamoylmethylphosphine Oxide for Understanding Its Extraction in Reprocessing Spent Nuclear Fuels. *Chem. - Eur. J.* **2011**, *17*, 13206−13216.
(41) Alvarez de Eulate, E.; Qiao, L.; Scanlon, M. D.; Girault, H. H.; Arrigan, D. W. M. Fingerprinting the tertiary structure of electroadsorbed lysozyme at soft interfaces by electrostatic spray ionization mass spectrometry. *Chem. Commun.* **2014**, *50*, 11829−11832.
(42) Liu, S.; Yu, Z.; Qiao, L.; Liu, B. Electrochemistry-mass spectrometry for mechanism study of oxygen reduction at water/oil interface. *Sci. Rep.* **2017**, *7*, 46669.

DOI: 10.1021/jacs.9b06299
J. Am. Chem. Soc. 2019, 141, 13212−13221

(43) Li, A.; Hollerbach, A.; Luo, Q.; Cooks, R. G. On-Demand Ambient Ionization of Picoliter Samples Using Charge Pulses. *Angew. Chem., Int. Ed.* **2015**, *54*, 6893−6895.
(44) Hatay, I.; Su, B.; Li, F.; Mendez, M. A.; Khoury, T.; Gros, C. P.; Barbe, J. M.; Ersoz, M.; Samec, Z.; Girault, H. H. Proton-Coupled Oxygen Reduction at Liquid-Liquid Interfaces Catalyzed by Cobalt Porphine. *J. Am. Chem. Soc.* **2009**, *131*, 13453−13459.
(45) Fermin, D. J.; Dung Duong, H.; Ding, Z.; Brevet, P. F.; Girault, H. H. Photoinduced electron transfer at liquid/liquid interfaces - Part II. A study of the electron transfer and recombination dynamics by intensity modulated photocurrent spectroscopy (IMPS). *Phys. Chem. Chem. Phys.* **1999**, *1*, 1461−1467.
(46) Beattie, P. D.; Delay, A.; Girault, H. H. Investigation of the Kinetics of Assisted Potassium-Ion Transfer by Dibenzo-18-Crown-6 at the Micro-Ities by Means of Steady-State Voltammetry. *J. Electroanal. Chem.* **1995**, *380*, 167−175.
(47) Shao, Y.; Mirkin, M. V. Voltammetry at micropipet electrodes. *Anal. Chem.* **1998**, *70*, 3155−3161.
(48) Tong, Y.; Sun, P.; Zhang, Z.; Shao, Y. Fabrication of agar-gel microelectrodes and their application in the study of ion transfer across the agar-water 1,2-dichloroethane interface. *J. Electroanal. Chem.* **2001**, *504*, 52−58.
(49) Trojánek, A.; Langmaier, J.; Samec, Z. Electrocatalysis of the oxygen reduction at a polarised interface between two immiscible electrolyte solutions by electrochemically generated Pt particles. *Electrochem. Commun.* **2006**, *8*, 475−481.
(50) Su, B.; Hatay, I.; Trojánek, A.; Samec, Z.; Khoury, T.; Gros, C. P.; Barbe, J. M.; Daina, A.; Carrupt, P. A.; Girault, H. H. Molecular Electrocatalysis for Oxygen Reduction by Cobalt Porphyrins Adsorbed at Liquid/Liquid Interfaces. *J. Am. Chem. Soc.* **2010**, *132*, 2655−2662.
(51) Li, Y.; Wu, S.; Su, B. Proton-Coupled O_2 Reduction Reaction Catalysed by Cobalt Phthalocyanine at Liquid/Liquid Interfaces. *Chem. - Eur. J.* **2012**, *18*, 7372−7376.
(52) Fukuzumi, S.; Kotani, H.; Lucas, H. R.; Doi, K.; Suenobu, T.; Peterson, R. L.; Karlin, K. D. Mononuclear Copper Complex-Catalyzed Four-Electron Reduction of Oxygen. *J. Am. Chem. Soc.* **2010**, *132*, 6874−6875.
(53) Das, D.; Lee, Y. M.; Ohkubo, K.; Nam, W.; Karlin, K. D.; Fukuzumi, S. Acid-Induced Mechanism Change and Overpotential Decrease in Dioxygen Reduction Catalysis with a Dinuclear Copper Complex. *J. Am. Chem. Soc.* **2013**, *135*, 4018−4026.
(54) Pegis, M. L.; Wise, C. F.; Martin, D. J.; Mayer, J. M. Oxygen Reduction by Homogeneous Molecular Catalysts and Electrocatalysts. *Chem. Rev.* **2018**, *118*, 2340−2391.
(55) Fukuzumi, S.; Lee, Y. M.; Nam, W. Mechanisms of Two-Electron versus Four-Electron Reduction of Dioxygen Catalyzed by Earth-Abundant Metal Complexes. *ChemCatChem* **2018**, *10*, 9−28.
(56) Partovi-Nia, R.; Su, B.; Li, F.; Gros, C. P.; Barbe, J. M.; Samec, Z.; Girault, H. H. Proton Pump for O_2 Reduction Catalyzed by 5,10,15,20-Tetraphenylporphyrinatocobalt(II). *Chem. - Eur. J.* **2009**, *15*, 2335−2340.
(57) Xuan, Y.; Huang, X.; Su, B. Biomimetic Oxygen Reduction Reaction Catalyzed by Microperoxidase-11 at Liquid/Liquid Interfaces. *J. Phys. Chem. C* **2015**, *119*, 11685−11693.
(58) Fukuzumi, S.; Mochizuki, S.; Tanaka, T. Efficient Reduction of Dioxygen with Ferrocene Derivatives, Catalyzed by Metalloporphyrins in the Presence of Perchloric-Acid. *Inorg. Chem.* **1989**, *28*, 2459−2465.
(59) Fukuzumi, S.; Okamoto, K.; Gros, C. P.; Guilard, R. Mechanism of four-electron reduction of dioxygen to water by ferrocene derivatives in the presence of perchloric acid in benzonitrile, catalyzed by cofacial dicobalt porphyrins. *J. Am. Chem. Soc.* **2004**, *126*, 10441−10449.
(60) Chung, T. D.; Anson, F. C. Catalysis of the electroreduction of O_2 by cobalt 5,10,15,20-tetraphenylporphyrin dissolved in thin layers of benzonitrile on graphite electrodes. *J. Electroanal. Chem.* **2001**, *508*, 115−122.
(61) Peljo, P.; Murtomaki, L.; Kallio, T.; Xu, H. J.; Meyer, M.; Gros, C. P.; Barbe, J. M.; Girault, H. H.; Laasonen, K.; Kontturi, K. Biomimetic Oxygen Reduction by Cofacial Porphyrins at a Liquid−Liquid Interface. *J. Am. Chem. Soc.* **2012**, *134*, 5974−5984.

DOI: 10.1021/jacs.9b06299
J. Am. Chem. Soc. 2019, 141, 13212−13221